System for Robotically Assisted Prostate Biopsy and Therapy with Intraoperative CT Guidance[1]

Gabor Fichtinger, PhD, Theodore L. DeWeese, MD, Alexandru Patriciu, Attila Tanacs, Dumitru Mazilu, PhD
James H. Anderson, PhD, Ken Masamune, PhD, Russell H. Taylor, PhD, Dan Stoianovici, PhD

Rationale and Objectives. The purpose of this study was to assess the work-in-progress prototype of an image-guided, robotic system for accurate and consistent placement of transperineal needles into the prostate with intraoperative image guidance inside the gantry of a computed tomographic (CT) scanner.

Materials and Methods. The coach-mounted system consists of a seven-degrees-of-freedom, passive mounting arm; a remote-center-of-motion robot; and a motorized, radiolucent needle-insertion device to deliver 17–18-gauge implant and biopsy needles into the prostate with the transperineal route. The robot is registered to the image space with a stereotactic adapter. The surgeon plans and controls the intervention in the CT scanner room with a desktop computer that receives DICOM images from the CT scanner. The complete system fits in a carry-on suitcase, does not need calibration, and does not utilize vendor-specific features of the CT scanner.

Results. In open air, the average accuracy was better than 1 mm at a 5–8-cm depth. In various phantoms, the average orientation error was 1.3°, and the average distance between the needle tip and the target was 2 mm.

Conclusion. Results of preliminary experiments indicate that this robotic system may be suitable for transperineal needle placement into the prostate and shows potential in a variety of other percutaneous clinical applications.

Key Words. Biopsy; Computed tomographic (CT) guidance; Image-guided surgery; Prostate cancer; Surgical robotics; Transperineal needle placement.

Adenocarcinoma of the prostate is an important health problem in the Western hemisphere. After cardiac diseases and lung cancer, metastatic prostate cancer is the third-leading cause of death among men older than 50 years in the United States. Because of the evolution in screening techniques, more cases are being diagnosed at the early stage, when patients are candidates for some form of minimally invasive, localized therapy. The traditional treatment modalities—radical prostatectomy and external-beam radiation therapy—have produced impressive long-term survival data, but the recently available 5- and 10-year data regarding patients treated with radioactive seed therapy suggest similar results in low-risk patients. Substantial technical expertise, however, including accurate seed placement and patient selection, is required to achieve such results.

Contemporary biopsy and intraprostatic delivery of therapeutic agents are performed primarily with transrectal ultrasonographic (US) guidance. This technique has been overwhelmingly successful, but alternative image-guidance modalities have also been reported, primarily for the treatment of patients who have previously undergone rectal surgery (1–5).

Acad Radiol 2002; 9:60–74

[1] From the Engineering Research Center, New Engineering Bldg, Room 315 (G.F., A.P., A.T., R.H.T.), Brady Urological Institute (T.L.D., A.P., D.M., K.M., D.S.), and Departments of Radiation Oncology (T.L.D.,) and Radiology (J.H.A.), Johns Hopkins University, 3400 North Charles St, Baltimore, MD 21218-2682; and the Graduate School of Engineering, The University of Tokyo, Japan (K.M.). Received July 10, 2001; revision requested September 5; revision received September 24; accepted September 25. Supported by the National Science Foundation under Engineering Research Center grant EEC9731478, AdMeTech, the Henry M. Jackson Foundation, the U.S. Army Medical Research and Material Command, the Japanese government under the grand JSPS-RFTF99I00904, and the Whiting School of Engineering at the Johns Hopkins University. **Address correspondence to** G.F.

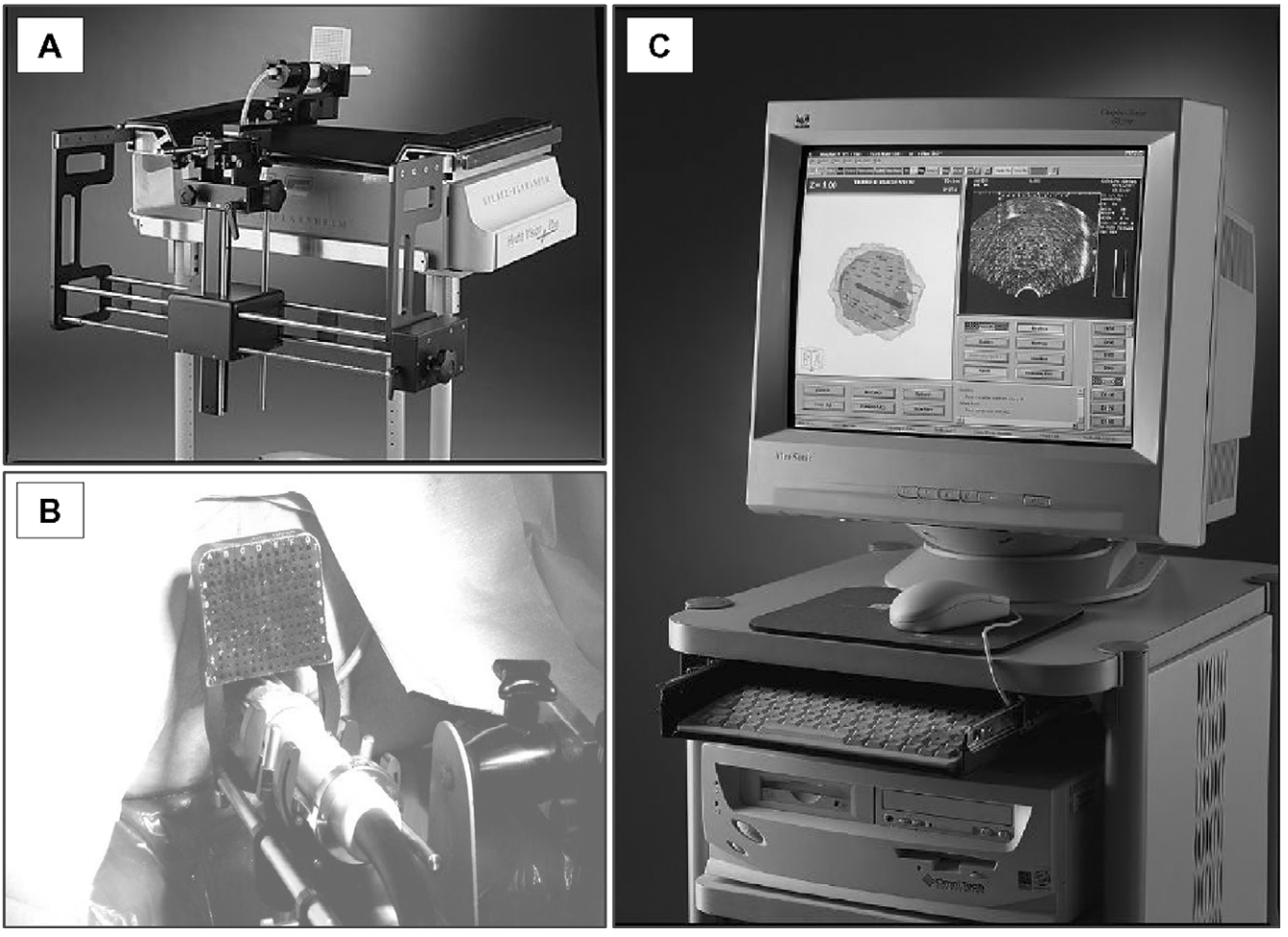

Figure 1. Standard transperineal prostate implant hardware. *A,* Table-mounted, stepping US probe and stationary template. *B,* Template fitted against the perineum with the transrectal US probe in place. *C,* Implant planning as performed on the computer. (Courtesy of Burdette Medical Systems, Champaign, Ill.)

With few exceptions, local therapies are delivered transperineally by using needles inserted through the holes of a template jig (Fig 1, *B*). Typically, the stepping transrectal US probe and stationary template jig are mounted on the end of the table (Fig 1, *A*). The patient is positioned in the lithotomy position, the template is fitted against the perineum, and the US probe is inserted into the patient's rectum (Fig 1, *B*). Planning for the implantation typically is carried out preoperatively on a computer receiving videostream images from the US unit. In the most recent systems, intraoperative planning has also been made available (Fig 1, *C*). The pattern of the jig dictates the direction and limits the possible locations of the needles, regardless of the condition presented by the individual patient.

Frequently, it is not possible to line up the template jig, US probe, and mounting hardware in such a way that the needles can reach potentially cancerous regions of the prostate that may be behind the pubic arch. This situation, which is commonly called "pubic arch interference," generally does not allow transperineal localized therapy to be performed. Koutrouvelis (4) has investigated alternative access routes to the prostate and found that a three-dimensional (3D), computed tomographic (CT)–guided, posterior ischiorectal approach is limited neither by the volume of the prostate and pubic arch interference nor by defects resulting from previous transurethral resection of the prostate. Although the posterior ischiorectal access has not been widely accepted, it represents an important step in the search for alternative solutions, and it proves

that CT is a suitable image-guidance modality for localized prostate therapy.

In many respects, the evolution of localized prostate therapies can be viewed as, in essence, an evolution of noninvasive visualization. If the implanted needles can be monitored accurately and their placement controlled as they release their payload inside the prostate, then it is theoretically possible to deposit the therapeutic agent (eg, ionizing radiation, heat, cold, genetic agents) while minimizing unwanted treatment of the surrounding normal tissue (eg, urethra). With the development of spatially accurate, real-time 3D hardware and software coupled with accurate, robot-augmented placement, this ideal can be achieved. Our approach to the problem was to maintain the largely successful transperineal access while replacing the manual technique with a robotic system for needle insertion that allows needles to enter at an arbitrary angle anywhere over the entire perineum. This solution offers numerous immediate and long-term advantages compared with the use of manually inserted, template-guided needles, including (*a*) elimination of the exclusion of patients on the basis of pubic arch interference, (*b*) consistent and precise needle delivery with robotic augmentation, (*c*) intraoperative 3D tracking of the implanted needles, (*d*) intraoperative updates of dosimetry and the implant plan itself, (*e*) full-scale exit dosimetry before the patient is released from the operating room, (*f*) intraoperative compensation for organ motion, deformation, and edema, and (*g*) reduction in radiation exposure of the operating-room team during brachytherapy.

Our ultimate goal is to develop clinical systems that use both transrectal US and CT guidance, but we selected CT as the guidance modality to be implemented first. This was primarily an engineering decision rather than an expression of any strong clinical preference.

Although CT might not be the optimal imaging modality for the prostate, it has many attractive features and advantages. It is a widely available and well-proven modality in planning electron-beam radiation therapy, which is often applied in combination with radioactive seed implants. Using CT imaging for both components of the treatment course may eliminate many of the registration problems that are involved with producing a combined radiation therapy plan. (Narayana et al [6] reported that prostate volume as determined with US typically was smaller than the preimplant volume as determined with CT.) Furthermore, a growing pool of patients with prostate cancer are being excluded from transrectal US because they have previously undergone rectal surgery. Historically, both transrectal US and CT guidance have been used during the delivery of radioisotopes into the prostate. Certainly, transrectal US is convenient for use in the standard operating-room environment, and it has a long record of successful application in this setting. Like transrectal US, CT produces transaxial images (typically at 5-mm intervals), but it also has the ability to simultaneously depict nonprostatic structures (eg, the pubic bone) that are not easily identified with transrectal US. This latter consideration can be particularly important in the delivery of seeds to the anterior portion of the prostate, thereby limiting the number of patients who are otherwise well suited for the standard transrectal US–guided approach. Moreover, CT is capable of producing images that are appropriate for proper anatomic identification and dosimetric planning considerations (4,5,7).

In comparison with transrectal US, CT has two obvious shortcomings: its lack of true real-time imaging and the toxic radiation that it delivers to the patient. These problems require use of a carefully crafted intraoperative imaging protocol. We would scan the treatment volume sparingly, but with a frequency that is sufficient to ascertain the correct needle position and dosimetry. In a clinical system, we plan to limit CT beam time by depicting the needles in batches; we will redepict the volume only after several needles have been inserted, but before their load is released. Use of CT is specifically advantageous for the localization of implanted needles and seeds, which allows us to update dosimetry intraoperatively. This also allows us to update the remaining part of the implant plan and to compensate for the dosimetric effects of misplaced seeds. Because the robotic system is no longer constrained to deliver needles along the holes of a template jig, we can also achieve arbitrary adjustments in the trajectory of the needles and deliver them with great accuracy. The absolute position of the needles and seeds is less important as long as the overall dosimetric coverage is guaranteed to be optimal.

From a systems engineering perspective, transrectal US and CT guidance for transperineal prostate access are similar in many ways. Both, for example, provide transaxial imaging with comparable spatial resolution. Many of the engineering details of the system can be worked out conveniently with the use of CT guidance, because CT permits more rapid prototyping, which later can be easily adapted to transrectal US guidance. Figure 2 shows the current CT-guided and the planned US-guided robotic systems, which apply essentially identical robotic hardware and overall systems architecture. An important point

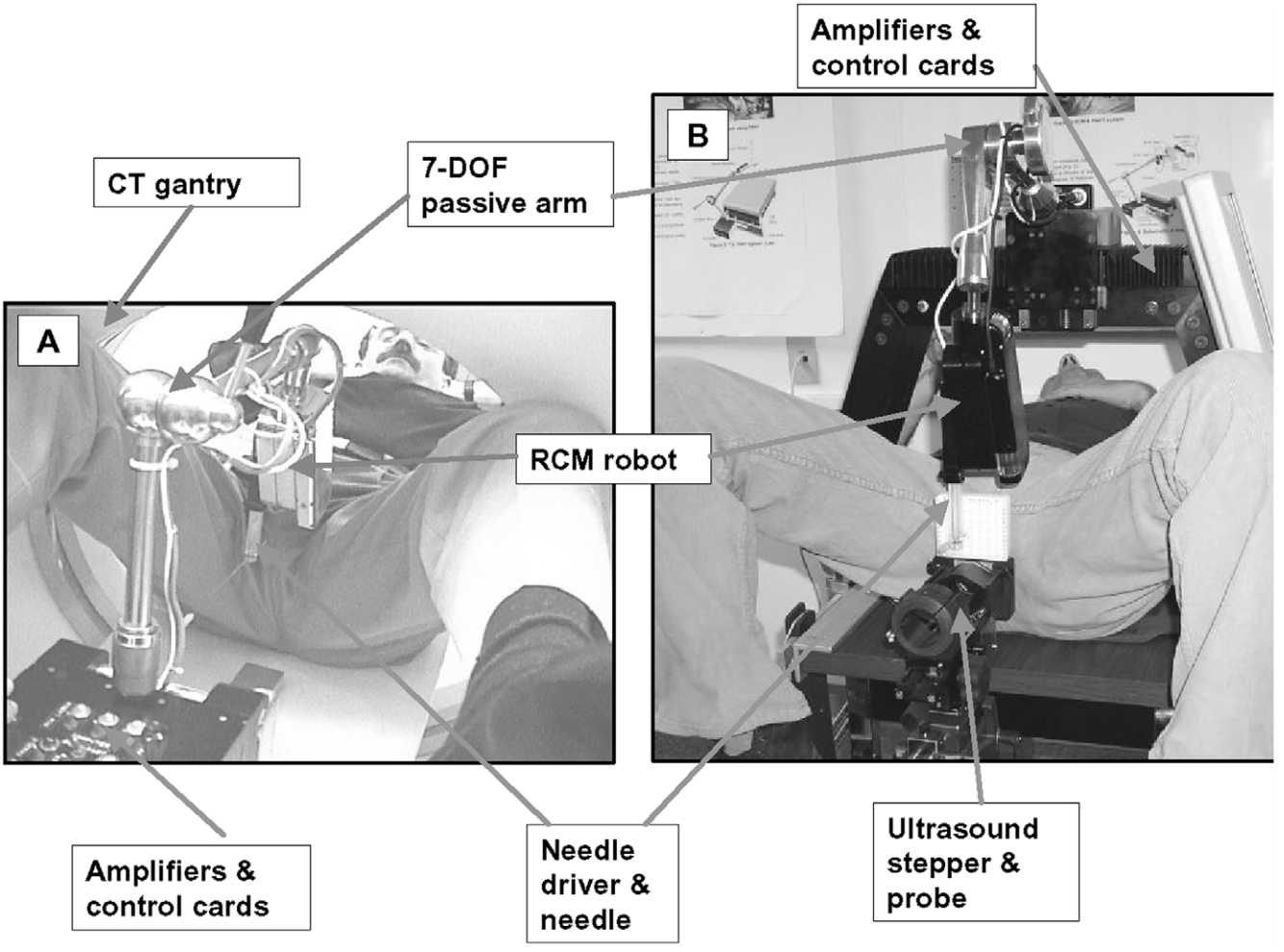

Figure 2. Current CT-guided and planned transrectal US–guided robotic systems for transperineal prostate access. The two systems employ identical robotic hardware and systems architecture. *A,* Patient in the treatment position inside the CT scanner. *B,* Patient in the treatment position with the US stepper and probe mounted in the standard position.

is that a CT-guided percutaneous system will be immediately applicable in other clinical procedures, as shown in Figure 3.

When considered from a larger perspective, one of the fundamental goals of our percutaneous research program at the Engineering Research Center is to develop modular and factorable image-guided robotic systems for surgery that, to a large extent, are invariant regarding the actual imaging modality with which they are deployed. Initially, we are focusing on solid-organ therapy, particularly of the prostate, but we plan to extend these results to other organ systems such as the brain, liver, and spine. These applications will involve an identical systems architecture and share many hardware and software components (8,9), although the physical embodiments of their robotic components may be grossly different. Percutaneous management of prostate cancer also fits naturally within the broader paradigm of "surgical computer-aided design (CAD)/computer-aided manufacturing (CAM)" systems as promoted by Taylor et al (10). The basic process of percutaneous local therapy involves two phases: first, planning a patient-specific pattern of therapy, which is analogous to CAD; and second, delivering the planned therapy through a series of percutaneous access steps, assessing the progress of the procedure, and using this feedback to control the process at several time scales, which is analogous to CAM.

The purpose of this study was to assess the work-in-progress prototype of an image-guided, robotic system for accurate and consistent placement of transperineal needles into the prostate with intraoperative image guidance inside the gantry of a CT scanner.

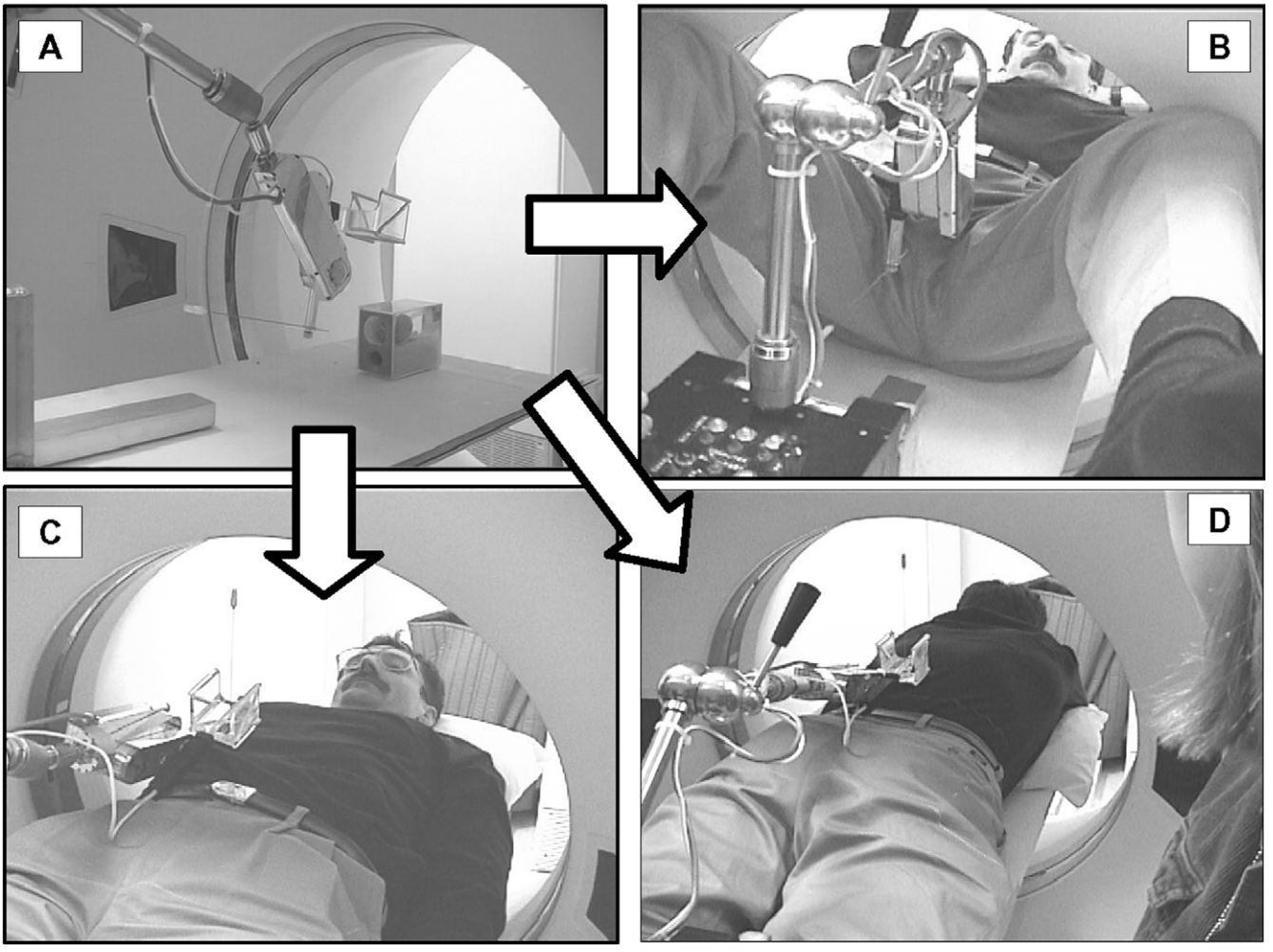

Figure 3. Transfer of robotic technology across clinical applications. The robotic system used in our initial phantom experiment *(A)* is easily deployed for applications involving the prostate *(B),* abdomen *(C),* and spine *(D).*

MATERIALS AND METHODS

Previous Engineering Art

Early experiences with CT-guided robots were associated with invasive head frames. On the basis of those principles, full-body stereotactic frames have been developed for abdominal and spinal access (11–13). Unfortunately, these systems are impractical for transperineal access in conjunction with the use of percutaneous robots. Masamune et al (14) detailed a coach-mounted, isocentric robot acting inside the CT gantry. This device was developed for intracranial neurosurgery, and it did not allow for the upward needle angles that are necessary to reach behind the pubic arch in the lithotomy position. Loser and Navab (15) developed a coach-mounted, in-CT, isocentric needle-insertion manipulator that was manually guided and that depended heavily on vendor-specific features of the scanner. A few commercial robotic needle-insertion systems also exist, such as the Neuromate robot (Integrated Surgical Systems, Davis, Calif). This robot has been approved by the U.S. Food and Drug Administration for stereotactic needle punctures, but it does not lend itself well to in-CT applications because of its large size and heavy weight. Stoianovici et al (16) have developed a compact and dexterous, remote-center-of-motion robot in conjunction with a radiolucent needle driver for percutaneous renal access under joystick control with C-arm fluoroscopy. This system is an excellent surgical aid, but it does not provide computerized remote control, which is necessary for computer-aided path planning and execution. Patriciu et al (17) have used the laser light of the CT scanner to register this same robot to the CT scanner

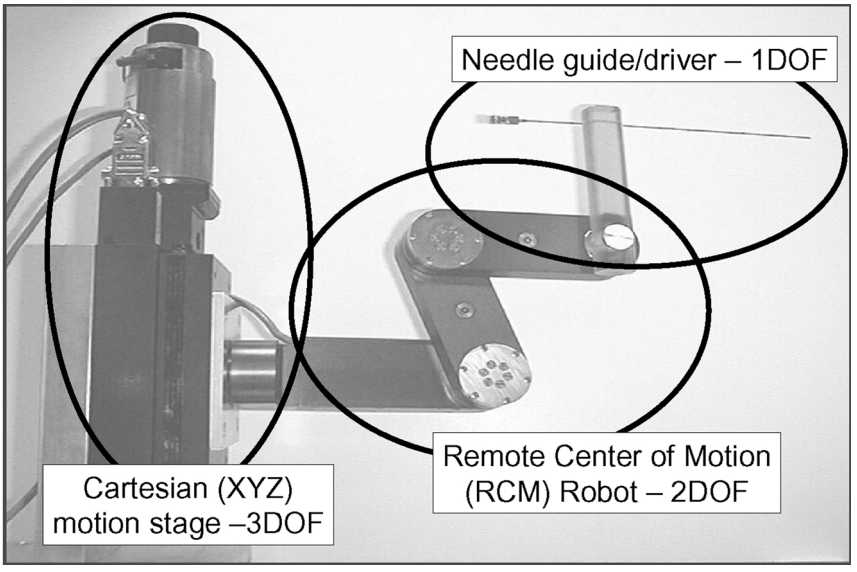

Figure 4. Basic robotic components assembled for percutaneous needle insertion. Before using this system, the tip of the needle must be positioned at the fulcrum point of the rotational stage. As illustrated here, the needle and its guide have not been adjusted to the center of motion.

and to achieve in-CT needle puncture. Susil et al (18) proposed a novel approach for registration of robotic manipulators to depict the space inside a CT scanner. Our solution has evolved along this line of research and, in essence, is an adaptation of the work by Stoianovici et al and Susil et al for transperineal access to the prostate by a plurality of needles.

Systems Description

Robotic components.—Manual needle punctures typically include three decoupled tasks: (*a*) touch-down of the needle tip on the skin entry point, (*b*) orientation of the needle by pivoting it around the skin entry point, and (*c*) insertion of the needle into the body along a straight trajectory. Inserting a needle into an arbitrary location requires six independent stages of motion, which are also called degrees of freedom (DOF). First, three independent Cartesian motions (3-DOF) are necessary to move the needle tip from its current location to the skin entry point. Then, two independent rotations (2-DOF) are necessary to aim the needle by pivoting it around a fulcrum point at the skin entry point. Finally, a one-directional translation motion (1-DOF) is necessary to insert the needle into the body through the skin.

This kinematic sequence can be achieved by using the basic robotic system shown in Figure 4. The robotic components have been developed by, primarily, Cadeddu et al (19,20) and Taylor et al (21) at the Johns Hopkins University. The system consists of a 3-DOF Cartesian motion stage, a 2-DOF rotational stage, and a 1-DOF needle-insertion stage. The motion stages are performed sequentially. Only one stage moves at a time; motion power is turned off on the two other inactive stages. This scheme prevents insertion of the needle before its proper alignment has been confirmed, and it also prevents an accidental change in the path of the needle during insertion. The stages are kinematically constrained, and each stage involves only one kind of motion. For example, the rotation stage cannot translate, and the translation stage cannot rotate. The system also applies a nonbackdrivable transmission that preserves its configuration when the robot is deactivated or in the event of a power failure.

Overtravel of the stages is also a concern, but this is addressed extensively in the control software and by placing hard-stop blocks on the hardware. For example, accidental overtravel of the needle can be prevented by placing a sterile clamp on the needle shaft above the driving gear at the maximum insertion depth. These safety features guarantee that the robotic system performs only the prescribed motion and that each component stays within the set kinematic constraints.

All motion stages are powered by direct-current motors. The remote-center-of-motion robot employs a miniature parallelogram structure that is driven by a chain drive

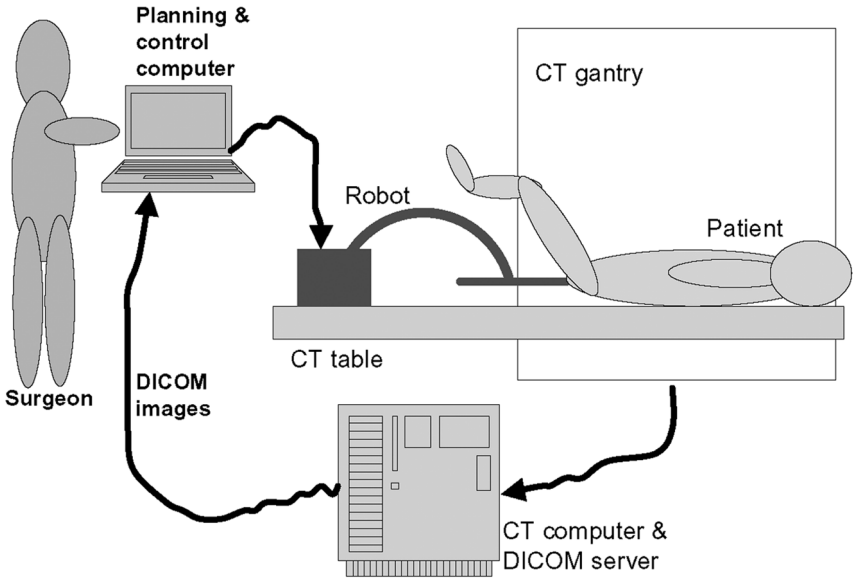

Figure 5. Schematic drawing of the prototype robotic system. The system implements a closed control loop in a simple "surgical CAD/CAM" scenario.

providing full 360° rotation around both axes. The needle-driver module employs the principle of friction transmission with axial loading (patent pending by Stoianovici, application serial no. 09/026,669). Both components have been used in multiple clinical scenarios at the Brady Urological Institute (19–21). The engineering characteristics of these devices have been published elsewhere (16).

The system applies purely image-based registration between the robot and the image space by applying a stereotactic frame that is permanently attached to the robot's end-effector. Registration and targeting are based on a single image section without the need for calibration, which promotes lower radiation exposure and a shorter procedure. The fundamentals of the registration have been published earlier by Susil et al (18).

Systems software and integration.—A schematic drawing of the overall configuration of the prototype system is presented in Figure 5. The CT scans are transferred across a local area network in DICOM (Digital Imaging and Communications in Medicine) format to a Pentium II, 333-MHz personal computer equipped with a 17-inch, flat-panel display. The computer runs a "simple storage" DICOM server, which was installed from a public domain source (22). The operator of the scanner pushes DICOM images from the CT console through the local area network to the DICOM server.

The central computer performs intraoperative image processing, motion planning, remote actuation, and control of the robotic components. These services are provided in the 3D Slicer software system, which was developed jointly with the Artificial Intelligence Laboratory at the Massachusetts Institute of Technology and the Surgical Planning Laboratory at the Brigham and Women's Hospital (8). With this software, the surgeon uses an interactive display to execute the intervention step by step (Fig 6). On completion of each step, the computer waits for confirmation before continuing. The interactive software completes an intraoperative control loop, thus implementing a simplified variant of the surgical CAD/CAM paradigm (10). Figure 6 also shows sample screens from the 3D Slicer–based path planning and visualization process. Stereotactic fiducials are picked, and the prostate is contoured semiautomatically (Fig 6). The robot and the patient are registered, and the path and the pattern of the needles are planned in three dimensions (Fig 6, *B*).

The robotic stages are controlled by the Modular Robot Control library, which was previously developed by Taylor et al (23) at the Johns Hopkins University. The MRC library, which is fully integrated with the 3D Slicer system, is a set of portable C++ classes for distributed and modular robotic control. Some of the functionality is limited to WIN32 operating systems, but most of the classes are independent of the specific operating system. The Modular Robot Control library provides Cartesian level control for serial manipulators with multi–priority level clients and multiclient servers for distributed robotic control. The control library includes classes for kinematics, joint level control, command and command table

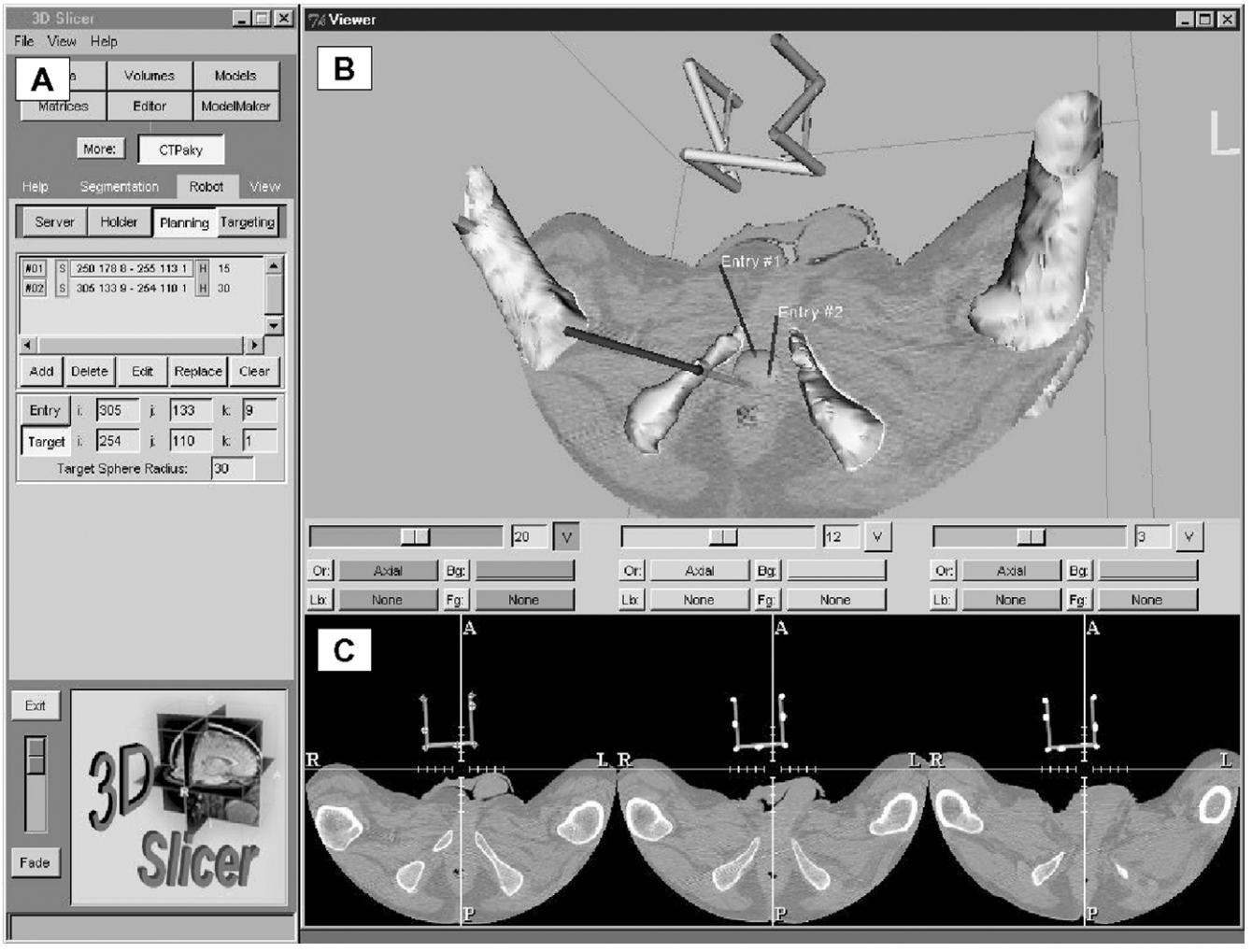

Figure 6. Control, visualization, and path planning in the 3D Slicer system. *A,* The 3D Slicer system is an interactive, Windows NT client application program. *B,* The robot and patient are coregistered, and then the path and the pattern of the needles are planned on a 3D model. *C,* Fiducials are picked, and the robot is registered to image space automatically.

management, sensor and peripheral support, and network and remote procedure call, or RPC, support. Limited exception and error handling are also built-in. An array of sensors using serial and parallel ports, including ATI force sensors (Apex, NC), joysticks, digital buttons, and foot pedals, are also supported. Support is also available for a variety of motion controllers, such as MEI cards (Santa Barbara, Calif) and the proprietary LARS servocontroller (IBM, Yorktown Heights, NY).

The central computer of the system also enables the gathering of complex intraoperative information. Postoperational processing of these data is expected to become valuable for outcome analysis, rehabilitation planning, and performance evaluation of the engineered system.

The system does not depend on any vendor-specific features of hardware or software. It can be used with any scanner that has a DICOM interface.

Prototype embodiment.—The actual preclinical prototype is shown in Figure 7, in which the robotic system is mounted on the CT coach. To promote the encapsulation of robotic components, the amplifiers and power supplies are built inside the robot mount. Temporarily, the Cartesian motion stage was replaced by an unencoded, passive mounting arm that locks and unlocks easily with use of a handle. The arm is unlocked, the robot is moved manually to the skin entry point, and the arm is then locked. The rotational stage is attached to the arm, and the radiolucent, motorized needle-insertion device (ie, needle driver) is linked to the rotational stage. The combined

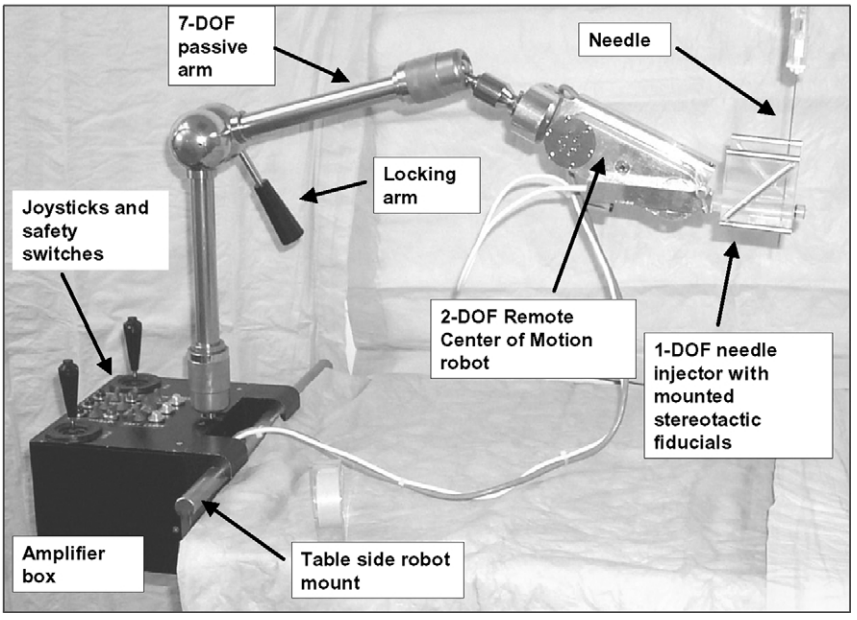

Figure 7. Preclinical robot assembly. The table-mounted system weighs only 15 kg and folds conveniently into a carry-on suitcase.

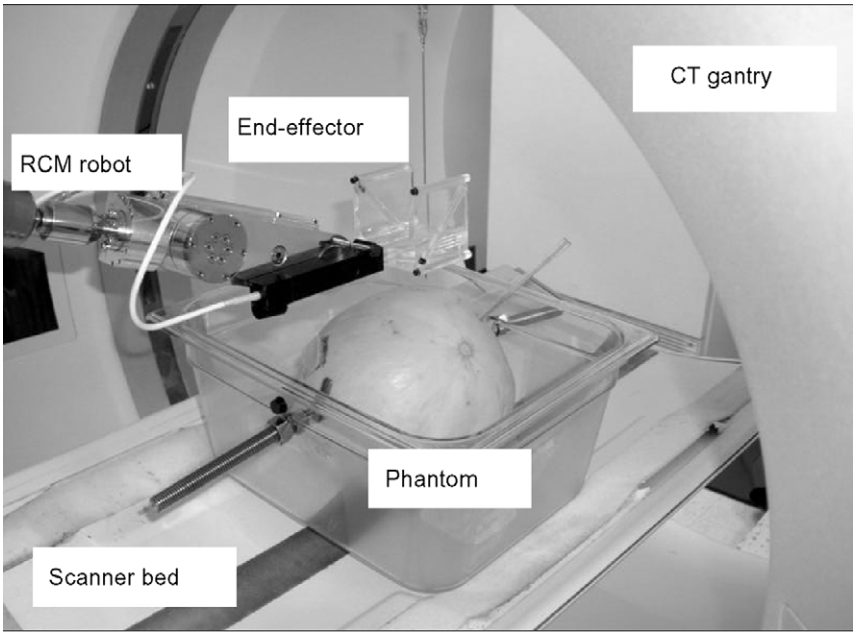

Figure 8. Phantom experiment with a honeydew melon. The melon, representing the patient, is placed in the CT scanner with the robot. *RCM* = remote center of motion.

weight of the system is approximately 15 kg. One reasonably skilled technician can set up and take down the system in 10 minutes. The entire robotic system, including the passive mount, rotational stage, and needle driver, folds conveniently into a carry-on suitcase.

Design of the Phantom Experiments

The phantom experiments were designed to prove the basic feasibility of this system. The specific goal was to demonstrate accurate needle placement in mechanical phantoms. An important objective also was to achieve an

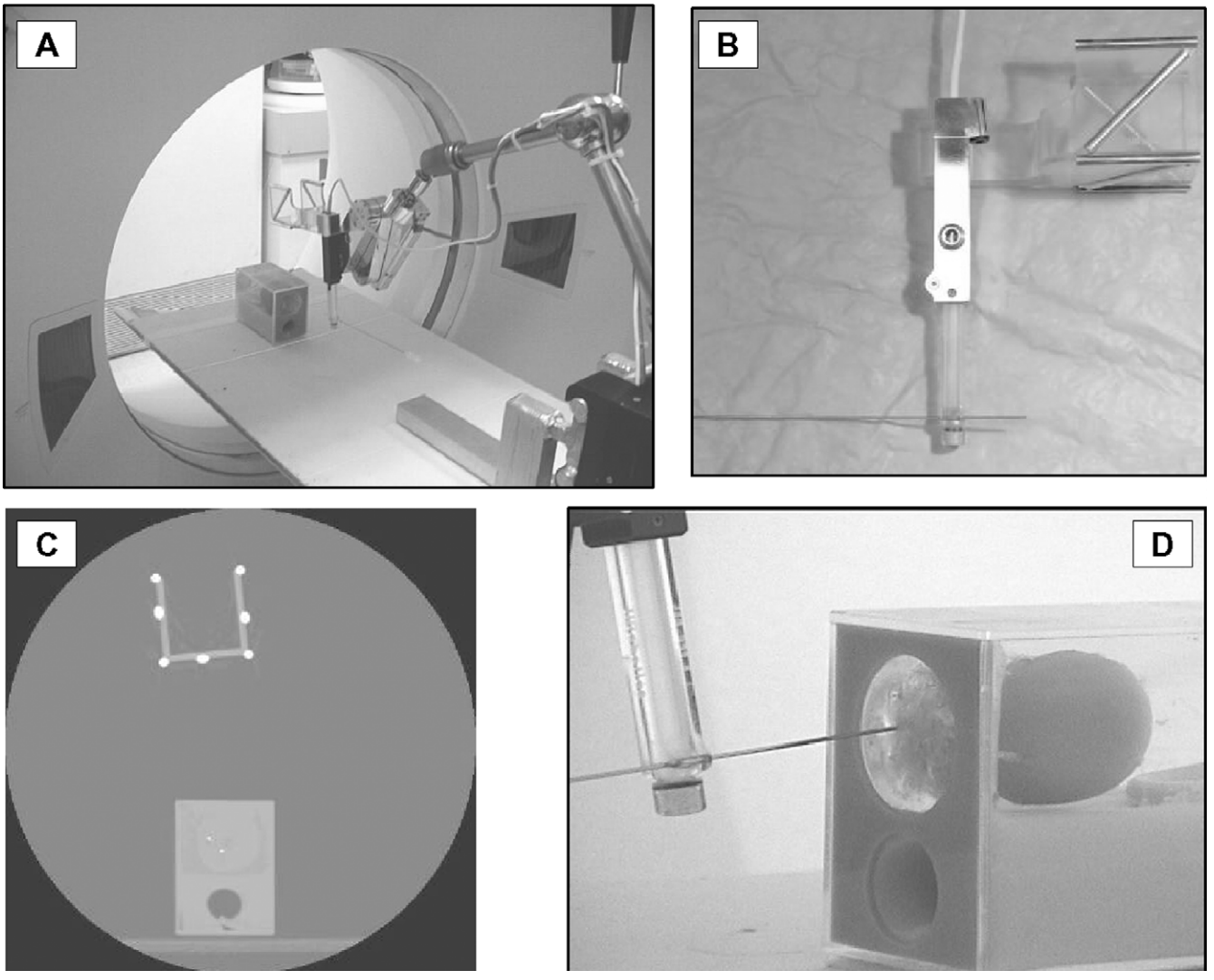

Figure 9. US training phantom experiment. *A,* The phantom and the robot mounted on the scanner table. *B,* Close view of the needle driver and the stereotactic end-effector frame. *C,* CT scan of the phantom and the stereotactic frame. *D,* Close view of a tilted needle being driven robotically into the phantom, thus demonstrating the capability of reaching behind the pubic arch.

upward needle trajectory, which will allow us to avoid interference with the pubic arch in clinical settings. We did not implant seeds or other objects into the prostate. We also did not intend to achieve a specific pattern of insertion.

To date, we have performed three sets of phantom experiments with this system. In the first set of experiments, a honeydew melon represented the patient (Fig 8). In the second, a standard, off-the-shelf prostate implant training phantom (Nuclear Associates, Hicksville, NY) was applied (Fig 9). In the third, actual clinical parameters were simulated with use of an anthropomorphic phantom. A full-body plaster cast of one of the investigators was produced, and a life-size torso with movable extremities was assembled from the cast. Finally, a prostate training phantom (Nuclear Associates) was inserted into the torso in such a way that the overall size and layout of organs reasonably represented that of an average male body (Fig 10).

The system was mounted inside the gantry of a CT scanner (GE Medical Systems, Waukesha, Wis). The targeting section thickness was 1.5 mm. Steel balls with a diameter of 2 mm were implanted into the phantoms and served as targets throughout the experiments. The targets were not inserted primarily in the central region of the phantoms, and they did not form any clinically mean-

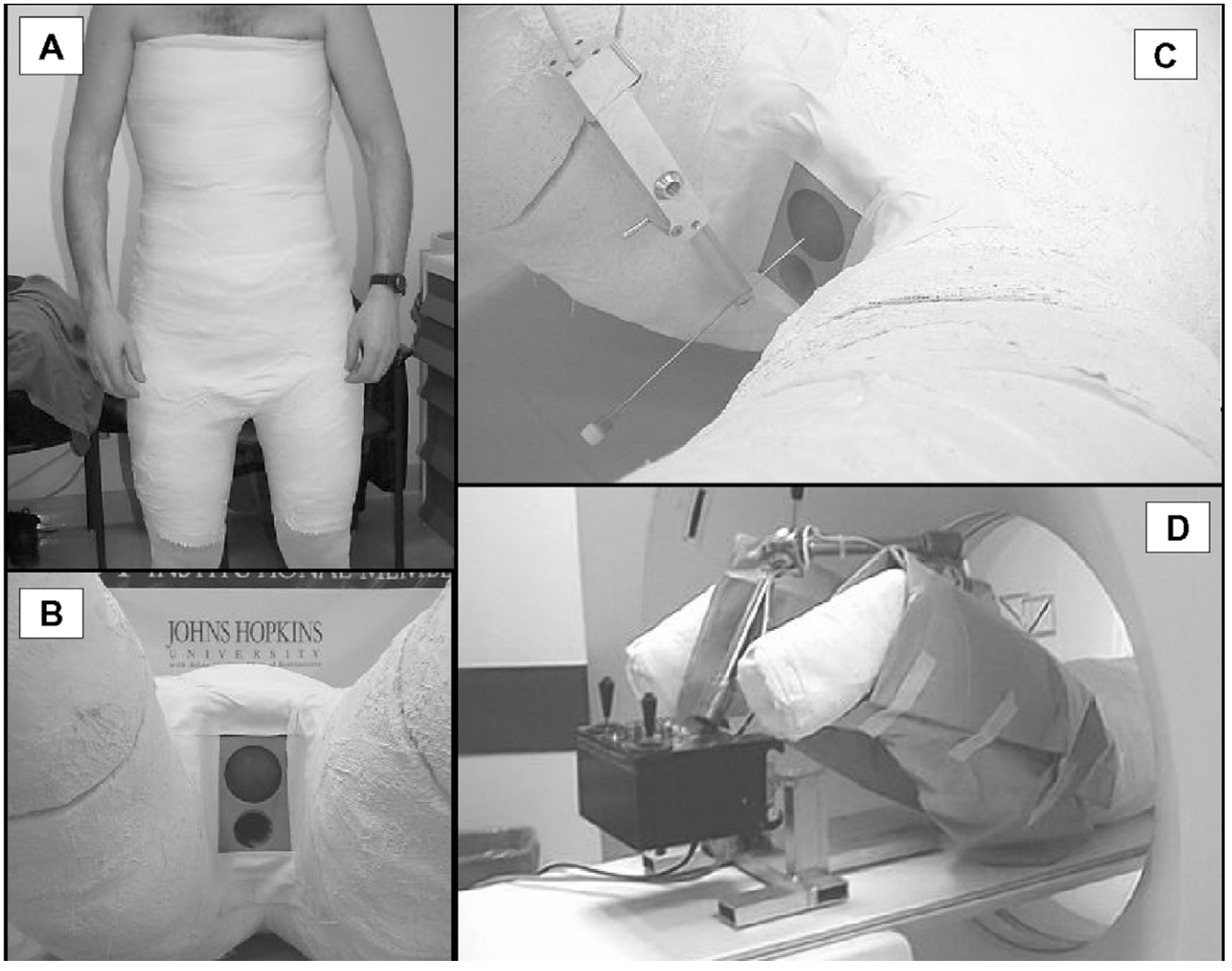

Figure 10. Anthropomorphic phantom experiment. *A,* Fabrication of a full-body phantom by making a plaster cast of a volunteer. *B,* US training phantom inserted in the pelvis of the plaster cast. *C,* Needle being driven robotically into the phantom through the perineum. *D,* Full-body phantom and robot mounted in the CT scanner.

ingful pattern. Standard 17-gauge, diamond-head needles were delivered to hit the implanted targets. Six needle insertions were performed in each set of experiments, and each insertion involved a slightly different access route.

The accuracy of needle placement is also associated with the speed of needle insertion. The maximum speed of the needle driver was 25 mm/sec, but we uniformly applied half-speed (ie, 12.5 mm/sec) throughout the experiments. The accuracy of needle placement was determined on the basis of 1-mm transaxial sections and scout images obtained with the same CT scanner without altering the position of the specimen.

RESULTS

In open air (ie, where no needle–tissue interaction occurs), we systematically achieved an average accuracy of 1 mm in hitting targets 5–8 cm from the fulcrum point.

In the melon experiment, the average orientation accuracy was 1°, whereas the average distance between the needle tip and the target was slightly more than 1.5 mm. A pair of confirmation images from the melon experiment are shown in Figure 11. In the transverse image, the tip of the needle accurately hits the target. In the corresponding projected scout view, a slight bending of the needle can also be observed.

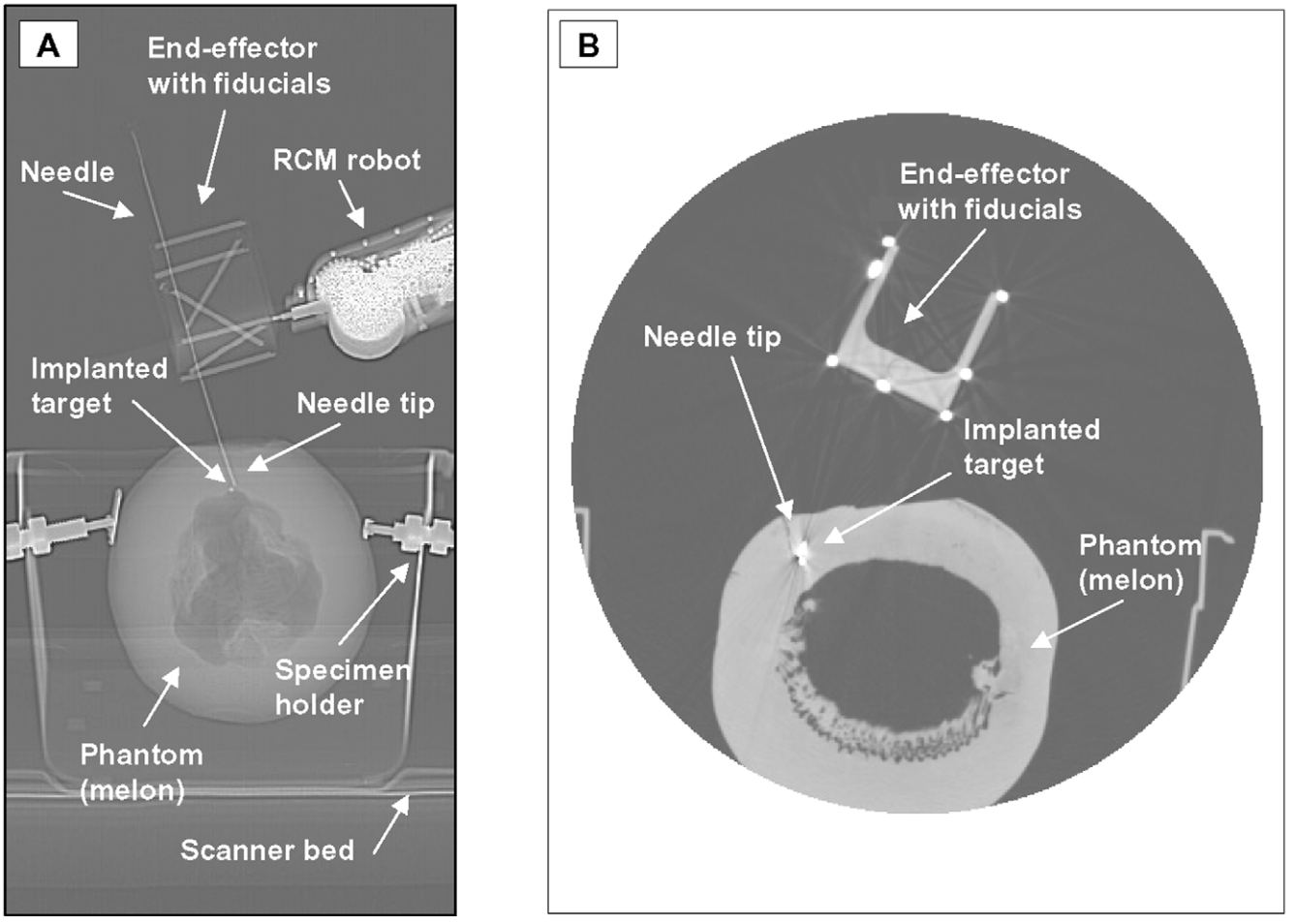

Figure 11. Confirmation CT scans of the honeydew phantom experiment. *A,* Scout view shows the target, needle, and robot. *RCM* = remote center of motion. *B,* CT scan shows the implanted target, needle tip, and stereotactic end-effector frame.

With the other two phantoms, somewhat less accurate results were achieved. The average orientation error was 1.6°, and the average distance between the needle tip and the implanted target was 2.5 mm. A pair of confirmation images for the prostate phantom are shown in Figure 12.

By selecting different entry points, arbitrarily tilted needle trajectories were achieved, including a slightly upward trajectory that indicates the ability to avoid pubic arch interference.

DISCUSSION

The results of the experiments suggested here suggest that the primary cause of needle-placement error is needle–tissue interaction. The overall accuracy in the phantom experiments was less than that achieved in the melon experiments, primarily because of needle deflection and tissue displacement. Ideally, the needle should be perpendicular to the skin surface to avoid transaxial slippage and deflection of the needle during penetration. Displacement of the prostate gland is expected to be more substantial in the human body; we plan to compensate for this by using bilateral stabilization needles. Inhomogeneities in the transperineal and prostatic tissues will also cause some additional error.

Our validation method was sufficiently accurate for use in a feasibility study of the robotic needle-insertion system, although the resolution (1.5-mm transaxial CT scans combined with scout views) did not allow submillimetric measurements to be obtained. In the human body, we expect to encounter somewhat larger errors than we saw in the homogeneous phantoms, so CT will remain our choice for future evaluations in cadavers and for in vivo experiments.

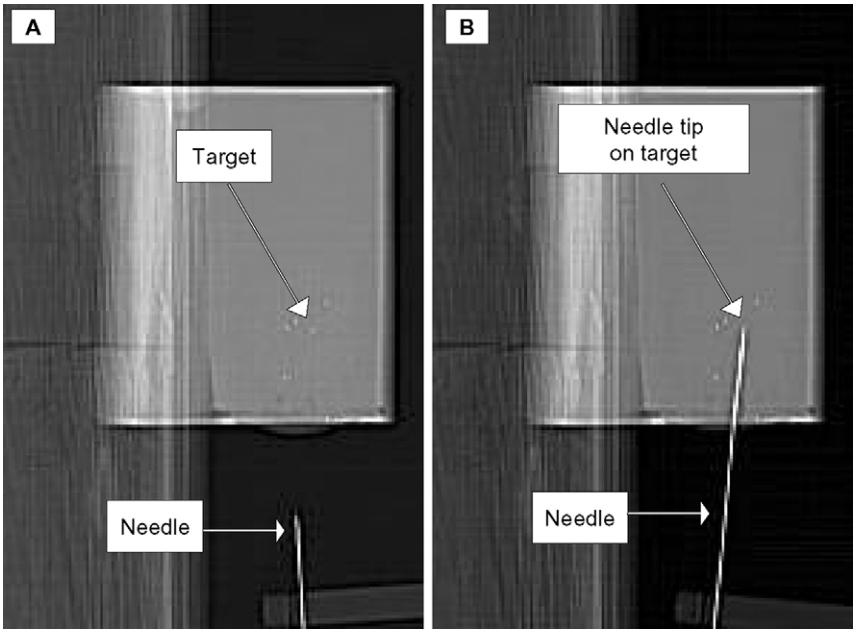

Figure 12. Confirmation x-ray images of the training phantom before and after needle insertion. *A,* Phantom with implanted metal targets before the experiment. *B,* Needle being driven accurately to the target.

Motion of the specimen obviously was not a problem in the phantom experiments. Currently, we assume that the patient would not move between acquisition of the targeting image and insertion of the needle; this appears to be a viable assumption in many cases. A full-fledged clinical system should be capable of detecting patient motion and of alerting the physician to this. If the patient moved, the robot could be rapidly reregistered to image space by acquiring a single CT scan. In another scenario, the robot could track and follow the motion of the treatment site. The added benefits of real-time compensation for patient motion must be carefully evaluated. In a laboratory setting, we have demonstrated that our 6-DOF robot can comply with the motion of the treatment site. This feature, however, requires real-time tracking hardware and complex motion-planning software, which add substantially to the overall complexity and cost of this system. Most important, 6-DOF compensatory robot motion requires simultaneous motion of all stages, which diminishes the safety of the decoupled stages. The effects of peristaltic movement could be eliminated by a rectal obturator, which would also have a positive side effect of stabilizing the prostate gland. Respiratory motion of the prostate in the lithotomy position is not expected to be an important factor.

The current needle driver uses friction transmission, which is associated with a maximum exertional force. If the resistance of the tissue is greater than the maximum transmission force, then the needle will slip axially and stop short of the target. We experienced occasional slippage of the needle in the phantom experiments. We detected friction by measuring the travel of the needle and then comparing it with the travel of the needle drive as known from the encoder. When slippage was detected, the experiment was rejected from the calculation of error. Interestingly, multiple insertions seemed to increase the likelihood of slippage, which was probably a result of the accumulation of fluids in the transmission mechanism during every retraction of the needle. To reduce axial slippage, we made a small incision on the surface of the phantom under the needle tip. Skin incision is not a viable clinical option, however, when multiple needles are delivered in a complex pattern. In response to this problem, a new needle driver with frictionless transmission has already been developed.

Upgrades of the robotic hardware will be necessary before the system can be used on humans. The current needle driver cannot release its grasp on the needle while the needle is inside the body, which is an important issue if involuntary movement of the patient is anticipated. The first prototype of a novel, frictionless needle driver with

needle-release and regrasp options has already been developed. Replacing the passive arm with an active, 3-DOF Cartesian motion stage is also in progress. Cartesian motion capability is required for delivering multiple needles in a complex pattern. In the improved system, the skin entry point will be picked from the CT scans, and the Cartesian stage will move the needle to the entry point. Clinical safety is a crucial issue, but one that could not be addressed in this article. Clinical trials with human subjects cannot be planned before a detailed safety evaluation regarding the entire system, including the robot, end-effector, and control software, is completed; such an evaluation is also in progress.

Although the number of needle insertions performed was limited in our feasibility experiments, they helped us to identify many important error factors. We made valuable observations that will be used in the design of further experiments with and improvements to this system.

In conclusion, we have demonstrated the technical feasibility of robotically assisted transperineal needle insertion inside a CT scanner. Results of experiments with mechanical phantoms indicate that this robotic system may be suitable for transperineal access to the prostate and, possibly, for a variety of other percutaneous clinical applications. Compared with other known robotic systems, our hardware system appears to be smaller, simpler, easier to use, and more cost-effective. Further experiments are needed, however, to evaluate the accuracy and safety of this system before it can be applied to human subjects.

ACKNOWLEDGMENTS

We are grateful to Faina Shtern, MD, president and chief executive officer of AdMeTech, who has been instrumental to our project since its early days. We gratefully acknowledge the long-standing support of Louis R. Kavoussi, MD, at the Brady Urological Institute, and we are also obliged to David M. Yousem, MD, for housing the experiments at the Division of Neuroradiology. Last, but not least, we are indebted to Vincent L. Lerie, RT, for spending many long hours with us in the scanner room—and without whom our research would not have been as much fun.

REFERENCES

1. Cormack RA, D'Amico AV, Hata N, Silverman S, Weinstein M, Tempany CM. Feasibility of transperineal prostate biopsy under interventional magnetic resonance guidance. Urology 2000; 56:663–664.
2. D'Amico A, Cormack R, Kumar S, Tempany CM. Real-time magnetic resonance imaging–guided brachytherapy in the treatment of selected patients with clinically localized prostate cancer. J Endourol 2000; 14: 367–370.
3. Cormack RA, Kooy H, Tempany CM, D'Amico AV. A clinical method for real-time dosimetric guidance of transperineal 125I prostate implants using interventional magnetic resonance imaging. Int J Radiat Oncol Biol Phys 2000; 46:207–214.
4. Koutrouvelis PG. Three-dimensional stereotactic posterior ischiorectal space computerized tomography guided brachytherapy of prostate cancer: a preliminary report. J Urol 1998; 159:142–145.
5. Arterbery VE, Wallner K, Roy J, Fuks Z. Short-term morbidity from CT-planned transperineal I-125 prostate implants. Int J Radiat Oncol Biol Phys 1993; 25:661–667.
6. Narayana V, Roberson PL, Pu AT, Sandler H, Winfield RH, McLaughlin PW. Impact of differences in ultrasound and computed tomography volumes on treatment planning of permanent prostate implants. Int J Radiat Oncol Biol Phys 1997; 37:1181–1185.
7. Roy JN, Wallner KE, Chiu-Tsao ST, Anderson LL, Ling CC. CT-based optimized planning for transperineal prostate implant with customized template. Int J Radiat Oncol Biol Phys 1991; 21:483–489.
8. Gering D, Nabavi A, Kikinis R, et al. An integrated visualization system for surgical planning and guidance using image fusion and interventional imaging. In: Proceedings of the second international conference on Medical Image Computing and Computer-Assisted Intervention, Cambridge, UK, 1999: lecture notes in computer science. Vol 1679. New York, NY: Springer, 1999; 809–819.
9. Schorr O, Hata N, Bzostek A, et al. Distributed modular computer-integrated surgical robotic systems: architecture for intelligent object. In: Proceedings of the third international conference on Medical Image Computing and Computer-Assisted Intervention, Pittsburgh, Pa, USA, 2000: lecture notes in computer science. Vol 1935. New York, NY: Springer, 2000; 969–987.
10. Taylor RH, Fichtinger G, Jensen P, Riviere C. Medical robotics and computer-integrated surgery: information-driven systems for 21st century operating rooms. J Jpn Soc Comput Aided Surg 2000; 2:47–53.
11. Erdi Y, Wessels B, DeJager R, et al. A new fiducial alignment system to overlay abdominal CT or MR images with radiolabeled antibody SPECT scans. Cancer 1994; 73:(suppl 3):923–931.
12. Takacs I, Hamilton AJ. Extracranial stereotactic radiosurgery: applications for the spine and beyond. Neurosurg Clin N Am 1999; 10:257–270.
13. Lohr F, Debus J, Frank C, et al. Noninvasive patient fixation for extracranial stereotactic radiotherapy. Int J Radiat Oncol Biol Phys 1999; 45:521–527.
14. Masamune K, Ji L-H, Suzuki M, Dohi T, Iseki H, Takakura K. A newly developed stereotactic robot with detachable drive for neurosurgery. In: Proceedings of the first international conference on Medical Image Computing and Computer-Assisted Intervention, Cambridge, Mass, USA, 1998: lecture notes in computer science. New York, NY: Springer, 1998; 215–222.
15. Loser M, Navab N. A new robotic system for visually controlled percutaneous interventions under CT. In: Proceedings of the third international conference on Medical Image Computing and Computer-Assisted Intervention, Pittsburgh, Pa, USA, 2000: lecture notes in computer science. Vol 1935. New York, NY: Springer, 2000; 887–897.
16. Stoianovici D, Cadeddu JA, Demaree RD, et al. An efficient needle injection technique and radiological guidance method for percutaneous procedures. In: Troccaz J, Grimson E, Mosges R, eds. Proceedings of CVRMed-MRCAS: lecture notes in computer science. Vol 1205. New York, NY: Springer, 1997; 295–298.
17. Patriciu A, Solomon S, Kavoussi L, Stoianovici D. Robotic kidney and spine percutaneous procedures using a new laser-based CT registration method. Presented at the Fourth International Conference on Medical Image Computing and Computer-Assisted Intervention (MICCAI), Utrecht, The Netherlands, October 14–17, 2001.
18. Susil RC, Anderson JH, Taylor RH. A single image registration method for CT-guided Interventions. In: Proceedings of the second interna-

tional conference on Medical Image Computing and Computer-Assisted Intervention, Cambridge, UK, 1999: lecture notes in computer science. Vol 1679. New York, NY: Springer, 1999; 798–808.
19. Cadeddu JA, Stoianovici D, Chen RN, Moore RG, Kavoussi LR. Stereotactic mechanical percutaneous renal access. J Endourol 1998; 12:121–126.
20. Cadeddu JA, Stoianovici D, Chen RN, Moore RG, Kavoussi LR. Mechanical percutaneous renal access. J Urol 1998; 159:110.
21. Taylor RH, Jensen P, Whitcomb LL, et al. A steady-hand robotic system for microsurgical augmentation. In: Proceedings of the second international conference on Medical Image Computing and Computer-Assisted Intervention, Cambridge, UK, 1999: lecture notes in computer science. Vol 1679. New York, NY: Springer, 1999; 1031–1041.
22. DICOM activities page. Electronic Radiology Laboratory, Mallinckrodt Institute of Radiology Web site. Available at: *http://www.erl.wustl.edu/DICOM/*. Accessed November, 2001.
23. CISST-ERC On-Line Documentation. Available at: *http://cisstweb.cs.jhu.edu/local/resources/software/mrc*. Accessed November 7, 2001.